

This is a postprint version of the following published document:

Moscoso, M., Novikov, A. and Papanicolaou, G.
(2016). Coherent Imaging without Phases. *SIAM J.
Imaging Sci.*, 9(4), 1689–1707

<https://doi.org/10.1137/16M1064830>

© 2016, Society for Industrial and Applied Mathematics

COHERENT IMAGING WITHOUT PHASES

MIGUEL MOSCOSO, ALEXEI NOVIKOV AND GEORGE PAPANICOLAOU

Abstract. In this paper we consider narrow band, active array imaging of weak localized scatterers when only the intensities are recorded at an array with N transducers. We consider that the medium is homogeneous and, hence, wave propagation is fully coherent. This work is an extension of our previous paper [21] where we showed that using linear combinations of intensity-only measurements, obtained from N^2 illuminations, imaging of localized scatterers can be carried out efficiently using imaging methods based on the singular value decomposition of the time-reversal matrix. Here we show the same strategy can be accomplished with only $3N - 2$ illuminations, therefore reducing enormously the data acquisition process. Furthermore, we show that in the paraxial regime one can form the images by using six illuminations only. In particular, this paraxial regime includes Fresnel and Fraunhofer diffraction. The key point of this work is that if one controls the illuminations, imaging with intensity-only can be easily reduced to a imaging with phases and, therefore, one can apply standard imaging techniques. Detailed numerical simulations illustrate the performance of the proposed imaging strategy with and without data noise.

Key words. array imaging, phase retrieval.

1. Introduction. In many situations it is difficult, or impossible, to measure the phases received at the detectors, only the intensities are available for imaging. This is the case, for example, in imaging from X-ray sources [20, 18, 22], or from optical sources [27, 10, 25], where one wants to form images from the spectral intensities. This is known as the phase retrieval problem, in which one seeks to reconstruct a complex signal from quadratic measurements involving the signal and, possibly, additional *a priori* information about it. The literature on the subject ranges from more or less sophisticated experimental setups that use interferometry to retrieve the phases [28, 9], to the use of algorithms that obtain the phases of the signals received at the array and then form the images [16, 15, 6, 5].

By far, the most popular methods for reconstructing a signal from only the magnitudes of its Fourier coefficients are alternating projection algorithms proposed by Gerchberg and Saxton [16] and later improved by Fienup [15]. These algorithms use a sequence of efficient projections in the Fourier and the spatial domains to reconstruct the missing phases of the Fourier coefficients that are consistent with their magnitudes and with the known spatial constraints. However, it is well known that these algorithms do not guarantee convergence, as they may suffer from stagnation of the iterates away from the true solution. In particular, they do not work well when prior knowledge about the sought signal is not available or is poor, and they often need a careful usage of the domain constraints (such as support and nonnegativity).

Another class of algorithms were proposed by Chai et. al. in [6] that framed the problem of array imaging using intensity-only measurements as a low-rank matrix completion problem. Motivated by the theory in compressed sensing, and in particular by the recent developments in matrix rank minimization theory [4], the authors in [6] replace the original non linear vector problem by a linear matrix problem with a rank-one solution. Since the resulting rank minimization problem is NP-hard, they relaxed it into a convenient convex program that seeks a low rank matrix that matches the intensity data by using nuclear norm minimization. A similar approach was used by Candes et. al. in [5] for diffraction imaging.

The main advantage of the approach in [6, 5] is that it guarantees exact recovery under some conditions on the imaging operator and the sparsity of the image. No additional constraints are needed on the image. However, the fact that a vector

problem is replaced by a matrix one makes the search of the solution very expensive if the images are large. Indeed, if the image is discretized using K pixels, then the reconstruction of the unknown image is done in a space of K^2 dimensions. This grand optimization problem is not feasible if, for example, a high resolution of the image is sought and, hence, the number of pixels is large.

The objective of this paper is to propose a new perspective for active array imaging of weak localized scatterers when only the intensities are available for imaging. We follow the same approach as in [21], where we came up with a new strategy that guarantees exact recovery and that is efficient for large scale problems. In [21], we showed that imaging with intensity-only measurements can be carried out by using an appropriate protocol of illuminations and the polarization identity. This allows us to obtain the time reversal operator of the imaging system. Once the time reversal operator has been obtained, the images can be formed using its singular value decomposition (SVD). This approach guarantees exact recovery of the image while keeping the computational cost low. However, the proposed strategy required N^2 illuminations and, therefore, the data acquisition process was expensive. In this paper we show that, in fact, only $3N - 2$ illuminations are needed, making the proposed approach in [21] feasible in practice.

We also consider the paraxial regime, which is the appropriate scaling for Fresnel or Fraunhofer diffraction. In this regime, array imaging has the form of a Fourier transform and, hence, the process of recovering an image is the classic phase retrieval problem. In this case, we show that only six illuminations are needed to create an image of a flat object. In our case, a flat object consists of a set of point-like scatterers located at the same range. The key point of the approach proposed here is that multiple versions of the intensity of the Fourier transform of an object, obtained through an appropriate set of illuminations, make the solution of the inverse problem of phase retrieval unique. We note, however, that the use of multiple measurements to resolve phase uniqueness is not new. Redundancy of the data to enforce phase uniqueness can be obtained, for example, by using random illuminations as in [13], or by inserting masks as in [5]. Another very interesting possibility is used in ptychography [26], a form of coherent diffractive imaging, where the object is stepped through a localized coherent wavefront generating a series of diffraction patterns. The illuminated area at each position overlaps with its neighbors and, thus, redundancy can be exploited during iterative phase-retrieval ptychography.

We also carry out numerical simulations that address the limitations of the proposed approach when the phaseless data is noisy. We find that sensitivity to noise is higher in the Fraunhofer regime when fewer illuminations are needed. That is the method of six illuminations, which is appropriate when the distance between the scatterers and the array is much larger than the wavelength of the signals and much larger than the linear dimensions of the array and the IW, is very sensitive to noise. This indicates that there is a trade-off between using a limited number of illuminations with phaseless data and the level of noise in the data.

The paper is organized as follows. In Section 2, we formulate the active array imaging problem using intensity-only measurements. In Section 3 we describe the illumination strategy and the imaging approach proposed in the paper. Section 4 contains our numerical simulations. The conclusions of this work are in Section 5.

2. Active array imaging. In active array imaging we seek to determine the location and reflectivities of a few reflectors by sending probing signals from an array and recording the backscattered signals. The active array \mathcal{A} consists of N transducers

placed at distance h between them. These transducers emit spherical wave signals from positions $\vec{\mathbf{x}}_s \in \mathcal{A}$ and record the echoes with receivers at positions $\vec{\mathbf{x}}_r \in \mathcal{A}$. In this paper, we consider narrow-band array imaging of sparse images consisting of a few point-like scatterers in a homogeneous medium. By point-like scatterers we mean very small scatterers compared to the wavelength of the probing signals. We assume that multiple scattering between the scatterers is negligible. For imaging problems with multiple scattering see [8].

FIG. 2.1. A general setup of array imaging problem

A typical configuration of the imaging setup of the array imaging problem is given in Figure 2.1. The active array has N transducers at positions $\vec{\mathbf{x}}_s$ located on the plane $z = 0$, so $\vec{\mathbf{x}}_s = (\mathbf{x}_s, 0)$, $s = 1, \dots, N$. There are M point-like scatterers in the image window (IW) that is discretized using a uniform grid of K points $\vec{\mathbf{y}}_j$, $j = 1, \dots, K$. The images are sparse because $K \gg M$. The scatterers with reflectivities $\alpha_j \in \mathbb{C}$ are located at positions $\vec{\boldsymbol{\xi}}_1, \dots, \vec{\boldsymbol{\xi}}_M$, which we assume coincide with one of these K grid points so $\{\vec{\boldsymbol{\xi}}_1, \dots, \vec{\boldsymbol{\xi}}_M\} \subset \{\vec{\mathbf{y}}_1, \dots, \vec{\mathbf{y}}_K\}$. For a study on imaging with ℓ_1 optimization when the scatterers lie off-grid we refer to [14, 1]. If the scatterers are far apart or the reflectivities are small, the interaction between them is weak and the Born approximation is applicable. In this case, the response at $\vec{\mathbf{x}}_r$ due to a narrow-band pulse of angular frequency ω sent from $\vec{\mathbf{x}}_s$ and reflected by the M scatterers is given by

$$P(\vec{\mathbf{x}}_r, \vec{\mathbf{x}}_s) = \sum_{j=1}^M \alpha_j G(\vec{\mathbf{x}}_r, \vec{\boldsymbol{\xi}}_j) G(\vec{\boldsymbol{\xi}}_j, \vec{\mathbf{x}}_s), \quad (2.1)$$

where

$$G(\vec{\mathbf{x}}, \vec{\mathbf{y}}) = \frac{\exp\{i\kappa|\vec{\mathbf{x}} - \vec{\mathbf{y}}|\}}{4\pi|\vec{\mathbf{x}} - \vec{\mathbf{y}}|} \quad (2.2)$$

is the Green's function that characterizes wave propagation from $\vec{\mathbf{x}}$ to $\vec{\mathbf{y}}$ in a 3-dimensional homogeneous medium. In (2.2), $\kappa = \omega/c_0$ is the wavenumber and c_0 is the wave speed in the medium. The nonlinear problem that includes multiple scattering between the scatterers is considered in [8].

To write the data received on the array in a more compact form, we define the *Green's function vector* $\mathbf{g}(\vec{\mathbf{y}})$ at location $\vec{\mathbf{y}}$ in IW as

$$\mathbf{g}(\vec{\mathbf{y}}) = [G(\vec{\mathbf{x}}_1, \vec{\mathbf{y}}), \dots, G(\vec{\mathbf{x}}_N, \vec{\mathbf{y}})]^t, \quad (2.3)$$

where \cdot^t denotes transpose. This vector represents the signal received at the array due to a point source at $\vec{\mathbf{y}}$. It can also be interpreted as the illumination vector of the array targeting the position $\vec{\mathbf{y}}$. We also introduce the true *reflectivity vector* $\boldsymbol{\rho} = [\rho_1, \dots, \rho_K]^t \in \mathbb{C}^K$ such that

$$\rho_k = \sum_{j=1}^M \alpha_j \delta_{\boldsymbol{\xi}_j, \mathbf{y}_k}, \quad k = 1, \dots, K, \quad (2.4)$$

where $\delta_{\cdot, \cdot}$ is the classical Kronecker delta. With this notation we can write the response matrix as a sum of rank-one matrices so

$$\mathbf{P} \equiv [P(\vec{\mathbf{x}}_r, \vec{\mathbf{x}}_s)]_{r,s=1}^N = \sum_{j=1}^M \alpha_j \mathbf{g}(\boldsymbol{\xi}_j) \mathbf{g}^t(\boldsymbol{\xi}_j) = \sum_{j=1}^K \rho_j \mathbf{g}(\boldsymbol{\xi}_j) \mathbf{g}^t(\boldsymbol{\xi}_j). \quad (2.5)$$

The entry $P(\vec{\mathbf{x}}_r, \vec{\mathbf{x}}_s)$ of this matrix denotes the signal received at $\vec{\mathbf{x}}_r$ due to a signal sent from $\vec{\mathbf{x}}_s$. Using (2.3), we also define the $N \times K$ sensing matrix

$$\mathcal{G} = [\mathbf{g}(\mathbf{y}_1) \cdots \mathbf{g}(\mathbf{y}_K)], \quad (2.6)$$

whose column vectors are the signals received at the array due to point sources at the grid points. Thus, \mathcal{G} maps a distribution of sources in the IW to the data received on the array. Using (2.6), we write (2.5) in matrix form as

$$\mathbf{P} = \mathcal{G} \text{diag}(\boldsymbol{\rho}) \mathcal{G}^t. \quad (2.7)$$

The full response matrix \mathbf{P} represents a linear transformation from the illumination space \mathbb{C}^N to the data space \mathbb{C}^N . Indeed, consider an illumination vector

$$\mathbf{f} = [f_1, \dots, f_N]^t,$$

whose components are the signals f_1, \dots, f_N sent from each of the N transducers in the array. Then, $\mathcal{G}^t \mathbf{f}$ gives the signals at each grid point of the IW. These signals are reflected by the scatterers on the grid that have reflectivities given by the vector $\boldsymbol{\rho}$, and then they are backpropagated to the array by the matrix \mathcal{G} . All the information available for imaging, including phases, is contained in the full response matrix \mathbf{P} . If sources and receivers are located at the same positions, then it is symmetric (due to Lorentz reciprocity) but not hermitian.

Given a set of illuminations $\{\mathbf{f}^{(j)}\}_{j=1,2,\dots}$, the usual imaging problem is to determine the location and reflectivities of the scatterers from the data

$$\mathbf{b}^{(j)} = \mathbf{P} \mathbf{f}^{(j)}, \quad j = 1, 2, \dots, \quad (2.8)$$

recorded at the array, including phases. If phase information is not available because only the intensities $\beta_i^{(j)} = |b_i^{(j)}|^2$ of the signals, $i = 1, \dots, N$, are recorded at the array, the imaging problem is to determine the location and reflectivities of the scatterers from the absolute values of each component in (2.8), i.e., from the intensity vectors

$$\boldsymbol{\beta}^{(j)} = \text{diag} \left(\left(\mathbf{P} \mathbf{f}^{(j)} \right) \left(\mathbf{P} \mathbf{f}^{(j)} \right)^* \right), \quad j = 1, 2, \dots, \quad (2.9)$$

where the superscript $*$ denotes conjugate transpose.

3. Coherent illuminations. The essential point in active array imaging of scatterers is that it is possible to control the illuminations to form the images. The main objective of this paper is to show that if one controls the illuminations the imaging problem with intensity-only can be reduced to one in which both intensities and phases are available and, therefore, algorithms that use the full dataset can be used to form the images. In this section, we show how to obtain the missing phases of the signals recorded at the array from linear combinations of the intensities of these signals. We first consider the general case in which sources and receivers are not placed at the same locations and, therefore, the response matrix of the imaging system is not symmetric. Then, we consider the typical imaging setup in which sources and receivers are located at the same positions and, therefore, the response matrix is symmetric. We finally consider the important case of Fresnel and Fraunhofer diffraction, where wave propagation can be modeled by the paraxial approximation.

3.1. General case. In [21], we proposed a novel imaging strategy for the case in which only data of the form (2.9) are recorded at the array. The main idea behind that approach is to use the *time reversal operator* $\mathbf{M} = \mathbf{P}^* \mathbf{P}$ for imaging, which can be obtained from intensity measurements using an appropriate illumination strategy and the polarization identity. Here we show how to obtain \mathbf{M} for imaging using a much more efficient illumination strategy. We do not assume that the response matrix \mathbf{P} is symmetric and, therefore, sources and receivers do not need to be located at the same positions.

In [21] we showed how to obtain all the entries of the matrix \mathbf{M} using $O(N^2)$ illuminations, where N is the number of sources in the array. That method uses only the total power received by the entire array, and the following polarization identities

$$\operatorname{Re}(M_{ij}(\omega)) = \frac{1}{2} \left(\|\widehat{\mathbf{P}}(\omega) \widehat{\mathbf{e}}_{i+j}\|^2 - \|\widehat{\mathbf{P}}(\omega) \widehat{\mathbf{e}}_i\|^2 - \|\widehat{\mathbf{P}}(\omega) \widehat{\mathbf{e}}_j\|^2 \right) \quad (3.1)$$

$$\operatorname{Im}(M_{ij}(\omega)) = \frac{1}{2} \left(\|\widehat{\mathbf{P}}(\omega) \widehat{\mathbf{e}}_{i-ij}\|^2 - \|\widehat{\mathbf{P}}(\omega) \widehat{\mathbf{e}}_i\|^2 - \|\widehat{\mathbf{P}}(\omega) \widehat{\mathbf{e}}_j\|^2 \right), \quad (3.2)$$

where $\widehat{\mathbf{e}}_i = [0, 0, \dots, 1, 0, \dots, 0]^T$ is the illumination vector whose entries are all zero except the i -th entry which is 1. In (3.1)-(3.2),

$$\widehat{\mathbf{e}}_{i+j} = \widehat{\mathbf{e}}_i + \widehat{\mathbf{e}}_j, \quad \widehat{\mathbf{e}}_{i-ij} = \widehat{\mathbf{e}}_i - i\widehat{\mathbf{e}}_j.$$

If instead of using the total power measured at the array as in [21], we use the intensities of the signals measured at every receiver separately, then we can obtain \mathbf{M} with significantly fewer $O(N)$ illuminations. Observe that each entry of the *time reversal operator* $\mathbf{M} = \mathbf{P}^* \mathbf{P}$ can be written as

$$m_{ij} = \sum_{k=1}^N p_{ki} \bar{p}_{kj}.$$

In order to recover $p_{ki} \bar{p}_{kj}$ it suffices to know the amplitudes of the signals $|p_{ki}|$, $|p_{kj}|$, $k = 1, \dots, N$, and to find the *phase differences* $\arg p_{ki} - \arg p_{kj}$, $k = 1, \dots, N$. Here, $\arg p_{ki}$ denotes the unrecorded phase of signal measured at the i -th receiver when the k -th source emits a signal. The amplitudes are recorded using N illuminations $\widehat{\mathbf{e}}_i$, $i = 1, 2, \dots, N$, and the phase differences can be recovered as follows. Since

$$\arg p_{ki} - \arg p_{kj} = (\arg p_{k1} - \arg p_{kj}) - (\arg p_{k1} - \arg p_{ki}),$$

it suffices to find the phase differences $\arg p_{k1} - \arg p_{kj}$ for $j = 2, \dots, N$, which means that only the phase differences between the first column of \mathbf{P} and all the other columns are needed. If all $p_{k1} \neq 0$, these phase differences can be found from the $2N - 2$ illuminations $\widehat{\mathbf{e}}_{1+j}, \widehat{\mathbf{e}}_{1-ij}$, $j = 2, \dots, N$, and the polarization identities (3.1), (3.2). When the image is sparse, the assumption $p_{k1} \neq 0$ is not restrictive because of the uncertainty principle [11].

3.2. Symmetric case. When sources and receivers are located at the same positions, \mathbf{P} is symmetric. In this case, we can obtain the full response matrix \mathbf{P} , up to a global phase, from intensity measurements using also $O(N)$ illuminations. Indeed, once we find $\arg p_{ki} - \arg p_{kj}$ for all i, j, k , we also know $\arg p_{ik} - \arg p_{jk}$ for all i, j, k . Note that in the general case we did not recover \mathbf{P} itself, as we did not

need it to image the scatterers. Indeed, in the general case where \mathbf{P} is not symmetric we use \mathbf{M} instead, as these two matrices have the same right singular vectors and, therefore, the images can be formed using SVD-based methods.

We point out that by using $O(s)$ illuminations we can obtain $O(s^2)$ distinct entries of the matrix \mathbf{P} up to a global phase. The strategy is as follows. Suppose we want to recover the $s \times s$ upper left corner of \mathbf{P} , with $s = 3$. First, we illuminate with the illumination vector $\hat{\mathbf{e}}_1$, and we set $p_{11} = |p_{11}|$. This fixes the global phase. Then, we use the three illumination vectors $\hat{\mathbf{e}}_2$, $\hat{\mathbf{e}}_1 + \hat{\mathbf{e}}_2$, and $\hat{\mathbf{e}}_1 - i\hat{\mathbf{e}}_2$. Apart from recording $|p_{k2}|$, $k = 1, 2, \dots, N$, we also recover the relative phases $\arg p_{k1} - \arg p_{k2}$, $k = 1, 2, \dots, N$, using the polarization identity. In particular, since the phase $\arg p_{11} = 0$, we recover p_{12} with its phase and, since \mathbf{P} is symmetric, p_{21} is also recovered with its phase. Furthermore, since the relative phase $\arg p_{21} - \arg p_{22}$ is then recovered, we obtain p_{22} with its phase as well. Next, we use the illumination vectors $\hat{\mathbf{e}}_3$, $\hat{\mathbf{e}}_1 + \hat{\mathbf{e}}_3$, and $\hat{\mathbf{e}}_1 - i\hat{\mathbf{e}}_3$. Since $\arg p_{11} - \arg p_{13} = -\arg p_{13}$, we recover p_{13} with its phase. Again, using the symmetry of \mathbf{P} we also obtain p_{31} . Since we know at this point $|p_{32}|$, $|p_{33}|$, $\arg p_{31} - \arg p_{32}$, and $\arg p_{31} - \arg p_{33}$, the entire 3×3 upper left corner of \mathbf{P} is recovered. Proceeding analogously, we can obtain the $s \times s$ upper left corner of \mathbf{P} after $3s - 2$ illuminations (up to a global phase).

3.3. Paraxial Approximation. Here, we further specialize the illumination strategy for the setup in which the distance between the scatterers and the array is much larger than the wavelength of the signals used to probe the medium and much larger than the linear dimensions of the array and the IW. In this case, wave propagation can be modeled by the paraxial approximation which is relevant for (near-field) Fresnel and (far-field) Fraunhofer diffraction. We assume that all the scatterers are at the same range from the array so the images are flat, and that sources and receivers are located at the same positions so the full response matrix \mathbf{P} is symmetric. In this case, \mathbf{P} has, up to pre-factor and post-factor diagonal matrices, a simple structure. More specifically, it can be written as

$$\mathbf{P} = \mathbf{D}_{\text{receiver}} \mathbf{H} \mathbf{D}_{\text{source}}, \quad (3.3)$$

where $\mathbf{D}_{\text{receiver}}$ and $\mathbf{D}_{\text{source}}$ are matrices that only depend on the geometrical setup, and \mathbf{H} is a matrix with a simple form. In the one-dimensional problem in which we seek to image a set of scatterers on a line using a linear array, \mathbf{H} is approximately Hankel, i.e., it is a symmetric matrix that is approximately constant across the anti-diagonals. This special structure of the matrix \mathbf{P} allows us to further reduce the number of illuminations to six in the one-dimensional setup, and to twelve in the two-dimensional setup, independently of the size of the array.

In the Appendix A we show that when the IW is far enough from the array the full-response matrix (2.1) can be approximated by the paraxial model

$$P_{\text{parax}}(\vec{\mathbf{x}}_r, \vec{\mathbf{x}}_s) = C_r C_s \sum_{j=1}^K \tilde{\rho}_j e^{-i\kappa \frac{\langle \mathbf{x}_s + \mathbf{x}_r, \mathbf{y}_j \rangle}{L}}, \quad (3.4)$$

where $\vec{\mathbf{x}}_s = (\mathbf{x}_s, 0)$ and $\vec{\mathbf{x}}_r = (\mathbf{x}_r, 0)$ are the positions of the sources and the receivers, respectively, $\vec{\mathbf{y}}_j = (\mathbf{y}_j, L)$, $j = 1, \dots, K$ are the grid points of the discretized IW, and

$$\tilde{\rho}_j = \rho_j e^{i\kappa |\mathbf{y}_j|^2 / 2L}, j = 1, \dots, K, \quad (3.5)$$

are distorted reflectivities that only modify the phases of the original reflectivities by a factor that depends on their (unknown) cross-range positions \mathbf{y}_j , and on the

distance L between the array and the IW, which we assume to be known. In Eq. (3.4),

$$C_t = C(\mathbf{x}_t) = \frac{e^{i\kappa L} e^{i\kappa |\mathbf{x}_t|^2 / 2L}}{4\pi L}, \quad t = r, s, \quad (3.6)$$

are known factors that only depend on the geometrical setup (the layout of the transducers and the distance L). Then, the approximated response matrix (3.4) can be written as in (3.3) with diagonal matrices

$$\mathbf{D}_{\text{source}} = \mathbf{D}_{\text{receiver}} \equiv [D_{r,s}]_{r,s=1}^N, \quad D_{r,s} = \delta_{r,s} C_r.$$

Equation (3.4) shows that, in the paraxial regime, array imaging with a single illumination has the form of a Fourier transform. Through the introduction of the distorted reflectivities (3.5), it includes both the near-field Fresnel regime, for which the Fresnel number

$$F = \frac{a^2}{\lambda L} \quad (3.7)$$

is $O(1)$, and the far-field Fraunhofer regime, for which $F \ll 1$. In the Fraunhofer regime the extra factor in the distorted reflectivities (3.5) approaches to 1, which means that the propagating fronts, when viewed from the IW, are not spherical but planar.

Because the structure of the full-response matrix is easier to describe in the one-dimensional imaging setup, we consider now a linear array on the line $\vec{\mathbf{x}} = (x, 0, 0)$ and a set of scatterers on the line $\vec{\mathbf{x}}' = (x', 0, L)$, see Fig. 4.1 (b). Assume that the paraxial approximation holds so $P(x_r, x_s) = P_{\text{parax}}(x_r, x_s)$, and consider the processed data

$$H(x_r, x_s) = (C_r C_s)^{-1} P(x_r, x_s) = \sum_{j=1}^K \tilde{\rho}_j e^{-i\kappa(x_r+x_s)x'_j/L}, \quad (3.8)$$

where x'_j are the grid points of the image, $j = 1, \dots, K$. Then, for a fixed configuration of the scatterers the entries in (3.8) only depend on $x_r + x_s$. This shows that if the IW is far enough from the array, the data received on the array only depends on the sum $r + s$ and, therefore, the matrix

$$\mathbf{H} \equiv [H_{r,s}]_{r,s=0}^{N-1} = [\Xi_{r,s}]_{r,s=0}^{N-1} = \sum_{j=1}^K \tilde{\rho}_j e^{-i\Lambda \frac{(r+s)j}{N}}, \quad s, r = 0, \dots, N-1, \quad (3.9)$$

has constant skew-diagonals, i.e., \mathbf{H} is a Hankel matrix. In (3.9), we have defined the parameter

$$\Lambda = \frac{\kappa ab}{L K}, \quad (3.10)$$

where a and b are the lengths of the array and the IW, respectively. Note that Λ only depends on the imaging setup and the choice of discretization of the IW. For simplicity in (3.9), we have fixed the coordinate system so that $x_s = s a / N$, $s = 0, \dots, N-1$, $x_r = r a / N$, $r = 0, \dots, N-1$, $x'_j = j b / K$, $j = 1, \dots, K$.

Clearly, in the paraxial approximation, imaging is closely related to a discrete Fourier transform. In order to realize this connection, fix $s = 0$ and view $\mathbf{H} = \mathbf{H}(\tilde{\rho})$ as a linear map from the IW to the array, so

$$\mathbf{H} : \tilde{\rho} \rightarrow \sum_{j=1}^K \tilde{\rho}_j e^{-i \frac{\Lambda r_j}{N}}, r = 0, \dots, N-1. \quad (3.11)$$

The above is a Fourier transform if $N = K$ and $\Lambda = 2\pi$, which holds when the number of discrete points in the IW is $K = K_{opt} = ab(\lambda L)^{-1} = F b/a$, where F is the Fresnel number (3.7). We refer to K_{opt} as the optimal number of sampling points in the IW because for $N = K = K_{opt}$ (3.11) is an orthogonal transformation. Note that K_{opt} is the number of points in the IW if the sampling interval is the well known cross-range resolution limit $\lambda L/a$.

Note that since \mathbf{H} is a Hankel matrix, only two illuminations (from both edges of the array) are needed to obtain the full response matrix, if the phases can be recorded. All the other illuminations are redundant in the one-dimensional setup when the paraxial approximation holds and the scatterers are all at the same range.

Next, we show that six illuminations are enough to recover \mathbf{H} completely from intensity-only measurements. Let us assume that the phases cannot be measured and, therefore, only the intensities of the received signals are available for imaging. Let

$$\mathbf{f}^{(1)} = \mathbf{e}_1, \quad \mathbf{f}^{(2)} = \mathbf{D}_{source}^{-1} (\mathbf{e}_1 + \mathbf{e}_2), \quad \text{and} \quad \mathbf{f}^{(3)} = \mathbf{D}_{source}^{-1} (\mathbf{e}_1 + i\mathbf{e}_2),$$

with $\mathbf{e}_1 = [1, 0, 0, \dots, 0]^t$ and $\mathbf{e}_2 = [0, 1, 0, \dots, 0]^t$, be three illuminations that use the two top transducers of the array. When we use the above illuminations we measure

$$\text{diag} \left(\left(\mathbf{P} \mathbf{f}^{(1)} \right) \left(\mathbf{P} \mathbf{f}^{(1)} \right)^* \right) = \text{diag} \left(\left(\mathbf{H} \mathbf{e}_1 \right) \left(\mathbf{H} \mathbf{e}_1 \right)^* \right) = |\mathbf{h}^{(1)}|^2, \quad (3.12)$$

$$\text{diag} \left(\left(\mathbf{P} \mathbf{f}^{(2)} \right) \left(\mathbf{P} \mathbf{f}^{(2)} \right)^* \right) = |\mathbf{h}^{(1)} + \mathbf{h}^{(2)}|^2, \quad (3.13)$$

and

$$\text{diag} \left(\left(\mathbf{P} \mathbf{f}^{(3)} \right) \left(\mathbf{P} \mathbf{f}^{(3)} \right)^* \right) = |\mathbf{h}^{(1)} + i\mathbf{h}^{(2)}|^2, \quad (3.14)$$

respectively. In (3.12)-(3.14), $\mathbf{h}^{(1)}$ and $\mathbf{h}^{(2)}$ are the first and second columns of the matrix \mathbf{H} . Since \mathbf{H} is a Hankel matrix, (3.12), (3.13), and (3.14) are

$$|\mathbf{h}^{(1)}|^2 = \left[|\Xi_1|^2, |\Xi_2|^2, \dots, |\Xi_N|^2 \right]^t,$$

$$|\mathbf{h}^{(1)} + \mathbf{h}^{(2)}|^2 = \left[|\Xi_1 + \Xi_2|^2, |\Xi_2 + \Xi_3|^2, \dots, |\Xi_N + \Xi_{N+1}|^2 \right]^t,$$

and

$$|\mathbf{h}^{(1)} + i\mathbf{h}^{(2)}|^2 = \left[|\Xi_1 + i\Xi_2|^2, |\Xi_2 + i\Xi_3|^2, \dots, |\Xi_N + i\Xi_{N+1}|^2 \right]^t.$$

Using the polarization identity we can, therefore, obtain the dot products

$$\langle \Xi_i, \Xi_{i+1} \rangle, \quad i = 1, \dots, N,$$

from the intensities (3.12)-(3.14). Since $|\Xi_i|$ are known for $i = 1, 2, \dots, N$, we can retrieve Ξ_i , $i = 1, 2, \dots, N$ up to a common phase. Similarly, we can use the following three different illuminations

$$\mathbf{f}^{(4)} = \mathbf{e}_N, \mathbf{f}^{(5)} = \mathbf{D}_{\text{source}}^{-1} (\mathbf{e}_N + \mathbf{e}_{N-1}), \mathbf{f}^{(6)} = \mathbf{D}_{\text{source}}^{-1} (\mathbf{e}_N + i\mathbf{e}_{N-1}),$$

from the two transducers at the bottom of the array, to find the remaining Ξ_i for $i = N + 1, 2, \dots, 2N - 1$. If, for definiteness, we assume that Ξ_1 is a real positive number, then Ξ_i , $i = 1, 2, \dots, 2N - 1$ are determined uniquely, and therefore the matrix \mathbf{H} is reconstructed. Our construction again relies on the assumption that all $\Xi_i \neq 0$, which, as we mentioned earlier [11], is not restrictive.

The two-dimensional case consisting of a planar array and a planar image is analogous to the one described above. For a two-dimensional setup we will need to make twelve measurements to recover the full-response matrix instead of six as we showed in the one-dimensional setup.

4. Numerical Simulations. In this section we present numerical simulations that illustrate the performance of the proposed approach, where noise is also included. For simplicity of graphical representation we consider a linear array on the x axis. The scatterers lie either on the plane $(x, 0, z)$ as in Fig. 4.1 (a), in which case they are at different ranges from the array, or they lie on the line $(x, 0, L)$ as in Fig. 4.1 (b), in which case they are located at the same range L that we consider to be known. The coordinate system has origin at the center of the array and range axis z orthogonal to it. The relevant cross-range coordinate is, therefore, x . All the results presented here can be extended to the case in which one considers a planar square array and scatterers with cross-range coordinates (x, y) .

The linear array has aperture size $a = 2000\lambda$, and $N = 101$ transducers located at positions $(x_i, 0, 0)$, $i = 1, \dots, N$, that are 20 wavelengths apart. The scatterers, whose complex reflectivities are set randomly, are placed within a IW whose distance to the array vary from one numerical simulation to another. The IW is discretized using a uniform lattice with mesh size according to the distance L to the array. We choose the mesh size to be $h_z = \lambda L^2/a^2$ in the range direction, and $h_x = \lambda L/a$ in the cross-range direction. These are the well known resolutions limits in array imaging. Therefore, the smaller the distance between the array and the IW, the smaller the resolution is. To keep the number of grid points independent of the distance to the array we also change the size of the IW accordingly.

In all our numerical simulations the noise is modeled as additive. More specifically, the noise at the i -th receiver is modeled by adding a random variable ζ_i uniformly distributed on $[(1 - \varepsilon)\beta_i, (1 + \varepsilon)\beta_i]$, where β_i is the noiseless intensity received on the i -th receiver (see (2.9)), and $\varepsilon \in (0, 1)$ is a parameter that measures the noise strength. The noise added to the data gathered at different receivers when different illuminations are used is independent.

The left column of figure 4.2 shows three examples of sets of scatterers at distances $L = 2000\lambda$ (top row) and $L = 20000\lambda$ (middle and bottom row). The amplitudes and phases of the full response matrices \mathbf{P} are shown in the middle and right columns, respectively. All the information needed for imaging is encoded in these figures. However, in our case, phases are not available and, hence, the array imaging problem is to determine the configuration of the scatterers using only the amplitudes of the entries of \mathbf{P} , i.e., the middle column. For very large L (middle row), the paraxial approximation holds, and the \mathbf{P} matrix has a much simpler structure. If, in addition, all the scatterers are at the same range (bottom row), then the amplitude response

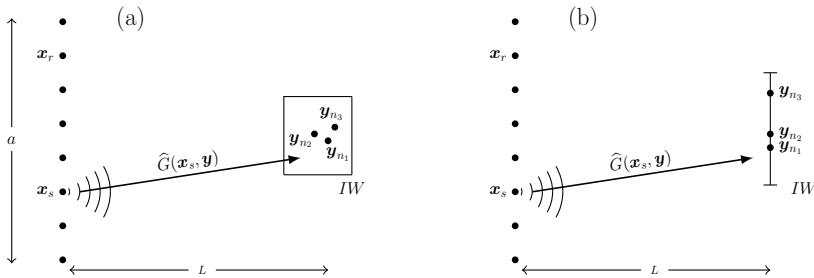


FIG. 4.1. Schematic. A linear array probes a homogeneous medium sending a spherical wave from \mathbf{x}_s . Wave propagation is described by the Green's function is $\hat{G}(\mathbf{x}_s, \mathbf{y})$. In figure (a) there are three point-like scatterers at positions \mathbf{y}_{n_j} , $j = 1, 2, 3$, whose ranges are different and unknown; the IW is a square. In figure (b), the point-like scatterers are on a line, and their range is unknown; the IW is a segment.

displays a Hankel structure. The phase response does not display a Hankel structure here, because the geometrical factors (3.6) (that are known) have not been removed.

Figure 4.3 displays the reference IW used for the numerical simulations in Figure 4.4. The scatterers are located at different ranges as in Fig. 4.1 (a). The range axes is in units of $h_z = \lambda L^2/a^2$, and the cross-range axes in units of $h_x = \lambda L/a$. This means that the resolution of the images increases as we move the IW forward. In Figure 4.4, the distance L between IW and the array is $L = 2000\lambda$ in the top row, $L = 5000\lambda$ in the middle row, and $L = 10000\lambda$ in the bottom row. The images are formed using the MUSIC (MUltiple SIgnal Classification) imaging function [23], reviewed in Appendix B, for the full time reversal matrix \mathbf{M} obtained with the illumination strategy described in subsection 3.1. The left column of Figure 4.4 shows the results for noise free data. We observe that by using MUSIC for \mathbf{M} we get the exact locations of the scatterers regardless of the distance between the array and the IW. As expected, when the data is corrupted by 10% (middle column) and 20% (right column) of additive noise the images become blurred and the resolution is compromised. We note, however, that all the scatterers are still very well resolved in cross-range.

To study the robustness of the proposed approach in the cross-range direction with respect to additive noise we consider flat images in Figure 4.5. By a flat image we mean that all the scatterers are placed at the same range L as in Fig. 4.1 (b), which we assume to be known. The unknown positions of the scatterers are $(x_i, 0, L)$, $i = 1, \dots, M$. The exact locations of the scatterers in these images are indicated with circles, and the peaks of the MUSIC pseudo-spectrum with stars. In the top row, the scatterers are placed at range $L = 10000\lambda$, in the middle one at $L = 20000\lambda$, and in the bottom one at $L = 50000\lambda$. The data used for the results in the left, middle and right columns contain 0%, 10%, and 30% of additive noise, respectively. Again, we obtain perfect cross-range positions when noiseless data is used. Furthermore, in the top row ($L = 10000\lambda$) all the peaks of the MUSIC pseudo-spectrum above the noise level correspond to scatterer locations. However, in the middle row ($L = 20000\lambda$) a few ghosts appear above the noise level when 30% of noise is added the data. In the bottom row ($L = 50000\lambda$) the ghosts appear above the noise level even with 10% of noise added to data. We conclude, as expected, that the robustness of the MUSIC algorithm is affected by the distance between the array and the IW. This is so because the larger the distance the flatter are the wavefronts that illuminate the IW.

In Figure 4.6, we show the results when wave propagation can be approximated

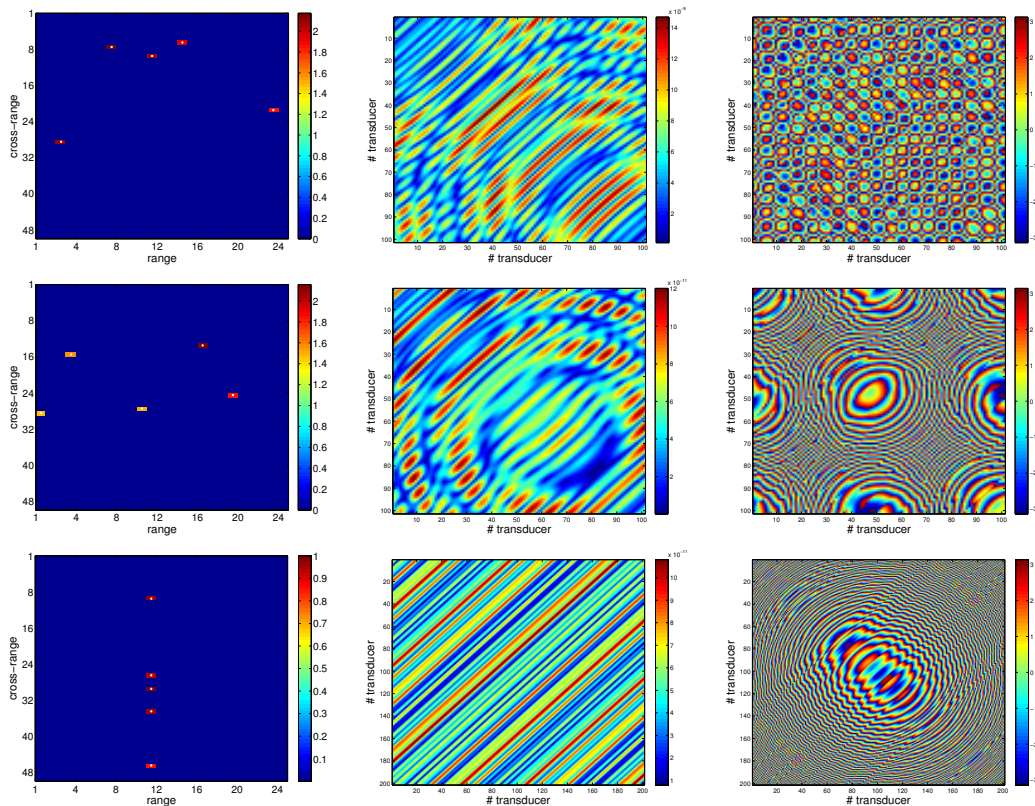


FIG. 4.2. Reference images (left column), and amplitudes (middle column) and phases (right column) of the response matrix P . The distances from the IWs to the array are $L = 2000$ (top row) and $L = 20000$ (middle and bottom row). In the left column, the range axes are in units of $h_z = \lambda L^2/a^2$ and the cross-range axes in units of $h_x = \lambda L/a$. The length of the array is 2000λ .

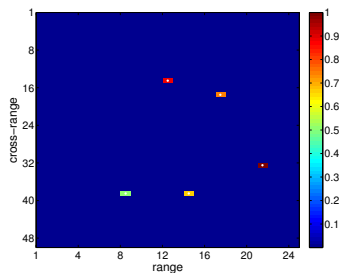


FIG. 4.3. Reference image used in Fig. 4.4. The range axis is in units of $h_z = \lambda L^2/a^2$ and the cross-range axis in units of $h_x = \lambda L/a$.

by the paraxial approximation and the full response matrix \mathbf{P} can be recovered, up to a global phase, using six illuminations as it is explained in subsection 3.3. In this figure, the scatterers are located on a line at range $L = 10000\lambda$ (first row), $L = 20000\lambda$ (second row), $L = 50000\lambda$ (third row), and $L = 100000\lambda$ (fourth row). The exact locations of the scatterers are indicated with circles, and the peaks of the MUSIC pseudo-spectrum of the recovered matrix \mathbf{P} with stars. The images shown

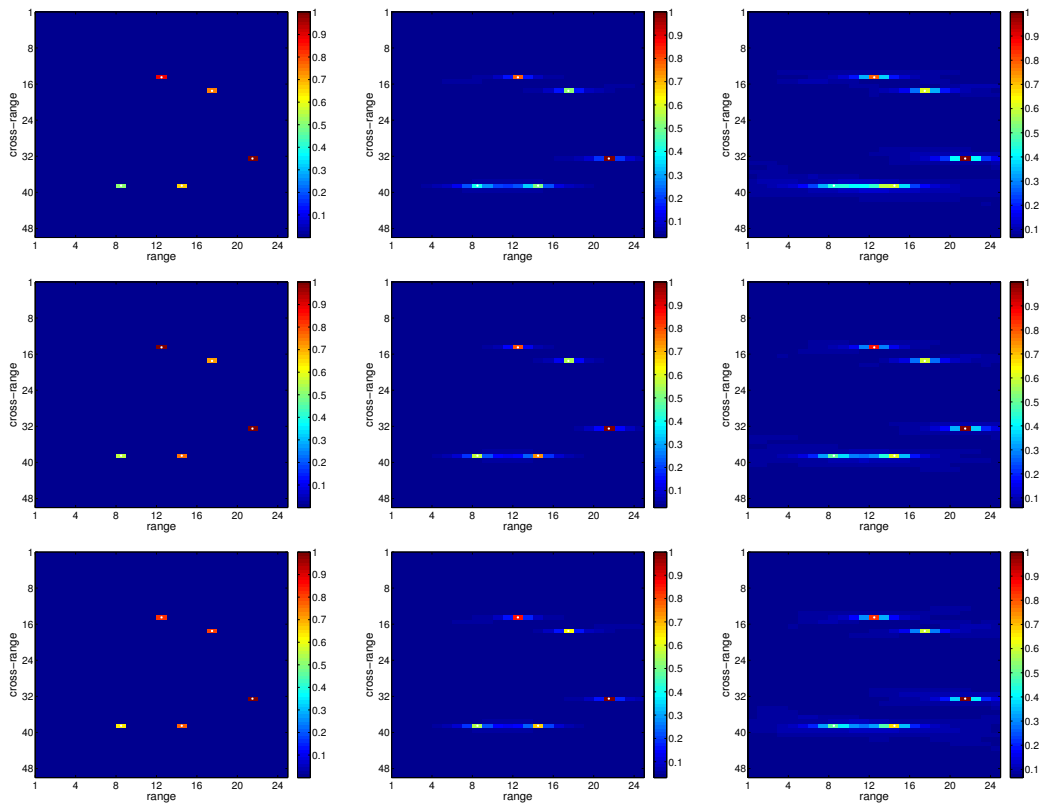


FIG. 4.4. Images obtained with MUSIC from the full recovered matrix M for different distances between the IW and the array. In the top, middle and bottom rows the distances between the IW and the array are $L = 2000\lambda$, $L = 5000\lambda$ and $L = 10000\lambda$, respectively. The left, middle and right columns contain 0%, 10%, 20% of additive noise in the data, respectively. Length of the array $a = 2000\lambda$, and number of transducers $Na = 101$. The range axes are in units of $h_z = \lambda L^2/a^2$ and the cross-range axes in units of $h_x = \lambda L/a$.

in the left, middle, and right columns are formed using data that contain 0%, 1%, and 10% of additive noise, respectively. The synthetic data is generated using (2.9), with \mathbf{P} given in (2.5), i.e., the data is not generated using the paraxial model (3.4). For noiseless data (left column), Figure 4.6 shows perfect reconstructions when the distances between the array and the IW are large enough (see the fourth and third rows for $L = 100000\lambda$ and $L = 50000\lambda$, respectively). However, the reconstructions become poor as we move the IW closer to the array (see the left column of the second and first rows for $L = 20000\lambda$ and $L = 10000\lambda$, respectively). This is due to modeling errors as the paraxial approximation deteriorates as we move the IW closer to the array. Because the distances between the array and the IW are very large, we also observe that the method is less robust with respect to additive noise. With 10% of noise the method fails to locate all the scatterers for all L (see the right column). Only for low level of noise and large enough L the method locates all the scatterers (see the middle column).

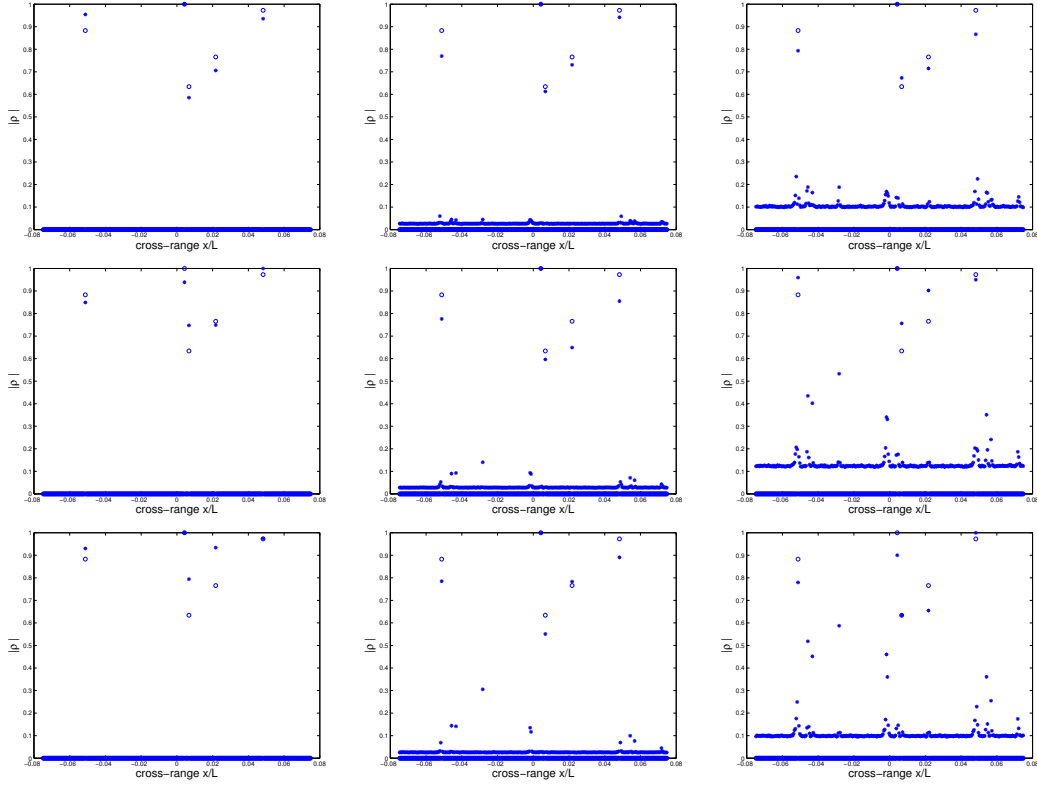


FIG. 4.5. Reconstructions obtained with MUSIC from the full recovered matrix M . In these numerical simulations the range L is assumed to be known. In the top, middle and bottom rows the ranges are $L = 10000\lambda$, $L = 20000\lambda$ and $L = 50000\lambda$, respectively. The left, middle and right columns contain 0%, 10%, and 30% of additive noise in the data, respectively. Length of the array $a = 2000\lambda$, and number of transducers $Na = 101$. The cross-range axes are in units of $h_x = \lambda L/a$.

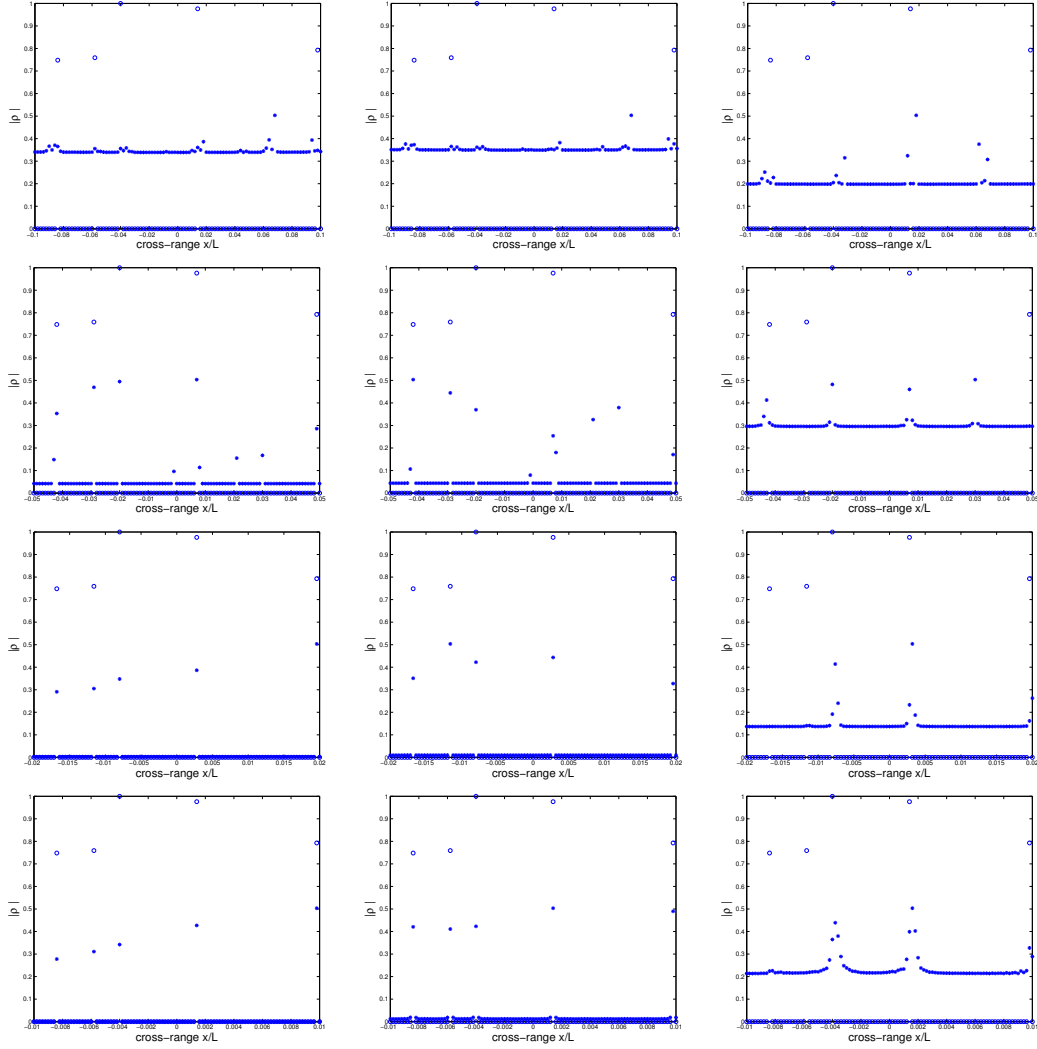


FIG. 4.6. Reconstructions obtained using MUSIC for the matrix \mathbf{P} recovered from six illuminations only. In the first, second, third, and fourth rows the distances between the array and the IW are $L = 10000\lambda$, $L = 20000\lambda$, and $L = 50000\lambda$, and $L = 100000\lambda$, respectively. The left, middle and right columns contain 0%, 1%, and 10% of additive noise in the data, respectively. The length of the array is $a = 2000\lambda$, and number of transducers is $Na = 101$. The cross-range axes are in units of $h_x = \lambda L/a$.

5. Conclusions. In this paper we consider narrow band, active array imaging of weak localized scatterers when only the intensities are recorded and measured at an array with N transducers. We assume that the medium is homogeneous so wave propagation is coherent. We show that if one controls the illuminations, the imaging problem with intensity-only can be easily reduced to one in which the phases are available. Furthermore, the amount of extra work in data acquisition is small, as only $3N - 2$ illuminations are needed in general. We also show that Fresnel and Fraunhofer diffraction images can be obtained by using only 6 illuminations for 1-D images and 12 illuminations for 2-D images, if these images are flat and their ranges are known.

Numerical simulations show the performance of the proposed approaches, with and without additive noisy in the data. The results presented in the paper indicate different noise sensitivities of these approaches. In particular, the method of six illuminations, that is valid when the distance between the scatterers and the array is much larger than the wavelength of the signals and much larger than the linear dimensions of the array and the IW, is very sensitive to noise. This limits the use of the six illuminations approach in practice to situations where the signal to noise ratio is high. Detailed analysis of robustness to noise with the proposed phaseless imaging methods is being considered at present.

Acknowledgment. Miguel Moscoso's work was partially supported by AFOSR FIS2013-41802-R and the Spanish MICINN grant FIS2013-41802-R. George Papanicolaou's work was partially supported by AFOSR grant FA9550-14-1-0275. Alexei Novikov's work was partially supported by AFOSR FIS2013-41802-R and NSF DMS-1515187.

Appendix A. Derivation of the paraxial approximation. Let the array be located on the plane $\vec{x} = (\mathbf{x}, 0)$ and the scatterers on the plane $\vec{y} = (\mathbf{y}, L)$. Then, we have

$$|\vec{x} - \vec{y}| = L \left(1 + \frac{1}{2} \left(\frac{|\mathbf{x} - \mathbf{y}|}{L} \right)^2 + O \left(\frac{|\mathbf{x} - \mathbf{y}|}{L} \right)^4 \right). \quad (\text{A.1})$$

If the distance L between the center of the array and the center of the IW is large enough and the linear dimensions of the array and the IW are small, so only the two first terms in (A.1) have to be retained, then (2.1) becomes

$$P(\mathbf{x}_r, \mathbf{x}_s) \approx P_{\text{parax}}(\mathbf{x}_r, \mathbf{x}_s) = \frac{e^{i2\kappa L}}{(4\pi L)^2} \sum_{j=1}^M \alpha_j e^{i\kappa [|\mathbf{x}_s - \boldsymbol{\xi}_j|^2 + |\mathbf{x}_r - \boldsymbol{\xi}_j|^2]/2L}, \quad (\text{A.2})$$

where $\boldsymbol{\xi}_j$ are the two-dimensional cross-range vectors that denote the scatterer's positions, and \mathbf{x}_s and \mathbf{x}_r are the two-dimensional cross-range vectors that denote the positions of the sources and the receivers, respectively. If we further expand the terms in the exponential, we obtain

$$P_{\text{parax}}(\mathbf{x}_r, \mathbf{x}_s) = C_r C_s \sum_{j=1}^M \bar{\alpha}_j e^{-i\kappa \frac{\langle \mathbf{x}_s + \mathbf{x}_r, \boldsymbol{\xi}_j \rangle}{L}} = C_r C_s \sum_{j=1}^K \tilde{\rho}_j e^{-i\kappa \frac{\langle \mathbf{x}_s + \mathbf{x}_r, \boldsymbol{\xi}_j \rangle}{L}}, \quad (\text{A.3})$$

where

$$\tilde{\rho}_j = \rho_j e^{i\kappa |\boldsymbol{\xi}_j|^2/2L} \quad (\text{A.4})$$

are distorted reflectivities that only change the phases of the reflectivities of the scatterers, and

$$C_t = C(\mathbf{x}_t) = \frac{e^{i\kappa L} e^{i\kappa|\mathbf{x}_t|^2/2L}}{4\pi L}, \quad t = r, s, \quad (\text{A.5})$$

are geometric factors that only depend on the imaging setup.

Equation (A.3) gives accurate results if the approximation in the phase for any two points $\vec{\mathbf{x}}$ and $\vec{\mathbf{y}}$ in the array and the IW is such that contribution of the third term in (A.1) is small, i.e., if

$$\frac{\kappa|\mathbf{x} - \mathbf{y}|^4}{8L^3} = \frac{\pi|\mathbf{x} - \mathbf{y}|^2}{4\lambda L} \left(\frac{|\mathbf{x} - \mathbf{y}|}{L} \right)^2 \ll \pi. \quad (\text{A.6})$$

Let a and b be two characteristic lengths of the array and the IW, respectively. Typically $a \leq b$, so $|\mathbf{x} - \mathbf{y}| \leq a$ for all \mathbf{x} and \mathbf{y} . Therefore, (A.3) models of wave propagation accurately if

$$\frac{1}{4}F \left(\frac{a}{L} \right)^2 \ll 1, \quad (\text{A.7})$$

where

$$F = \frac{a^2}{\lambda L} \quad (\text{A.8})$$

is the Fresnel number. In (A.2) and (A.3) we have kept the quadratic term of the expansion (A.1). In order for this term to be significant, we must have that $\frac{\kappa}{2} \frac{a^2}{L} \gtrsim \pi$, which means that

$$F \gtrsim 1 \quad (\text{A.9})$$

must hold. Conditions (A.7) and (A.9) characterize the Fresnel or near field regime. In this regime, the array does not have to be too small so the wave fronts appear to be planar when viewed from the array, as is the case in the Fraunhofer or far field regime. In the Fraunhofer regime we have the condition $F \ll 1$ instead, which means that the quadratic phase terms in (A.1) are negligible.

Appendix B. MUSIC. MUSIC is a subspace projection algorithm that uses the SVD of the full data array response matrix $\hat{\mathbf{P}}(\omega)$ to form the images. It is a direct algorithm widely used to image the locations of $M < N$ point-like scatterers in a region of interest. Once the locations are known, their reflectivities can be found from the recorded intensities using convex optimization as shown below.

Let us assume in this Section that $\hat{\mathbf{P}}(\omega)$ is fully recorded and known. We write the SVD of the data matrix $\hat{\mathbf{P}}(\omega)$ in the form

$$\hat{\mathbf{P}}(\omega) = \hat{\mathbf{U}}(\omega)\mathbf{\Sigma}(\omega)\hat{\mathbf{V}}^*(\omega) = \sum_{j=1}^{\tilde{M}} \sigma_j(\omega)\hat{U}_j(\omega)\hat{V}_j^*(\omega), \quad (\text{B.1})$$

where $\sigma_1(\omega) \geq \dots \geq \sigma_{\tilde{M}}(\omega) > 0$ are the nonzero singular values, and $\hat{U}_j(\omega)$, $\hat{V}_j(\omega)$ are the corresponding left and right singular vectors, respectively. They fulfill the following equations:

$$\hat{\mathbf{P}}^*(\omega)\hat{U}_j(\omega) = \sigma_j(\omega)\hat{V}_j(\omega), \quad \hat{\mathbf{P}}(\omega)\hat{V}_j(\omega) = \sigma_j(\omega)\hat{U}_j(\omega), \quad j = 1, \dots, N. \quad (\text{B.2})$$

Since $\widehat{\mathbf{P}}(\omega)$ is symmetric, $\widehat{U}_j(\omega) = e^{i\theta_j} \widehat{V}_j(\omega)$ for some unknown global phase θ_j , $j = 1, \dots, N$.

The search of the locations of the M scatterers is the combinatorial part of the imaging problem and, hence, by far the most difficult task. Note that $\widehat{\mathbf{P}}(\omega)$ is a linear transformation from the *illumination space* \mathbb{C}^N to the *data space* \mathbb{C}^N . According to (B.1), the illumination space can be decomposed into the direct sum of a signal space, spanned by the principal singular vectors $\widehat{V}_j(\omega)$, $j = 1 \dots, M$, having non-zero singular values, and a noise space spanned by the singular vectors having zero singular values. Since the singular vectors $\widehat{V}_j(\omega)$, $j = M + 1, \dots, N$, span the noise space, the probing vectors $\widehat{\mathbf{g}}_0(\mathbf{y}_j, \omega)$ will be orthogonal to the noise space only when \mathbf{y}_j corresponds to a scatterer's location \mathbf{y}_{n_j} . Hence, it follows that the scatterers' locations must correspond to the peaks of the functional

$$\mathcal{I}(\mathbf{y}_s) = \frac{1}{\sum_{j=M+1}^N |\widehat{\mathbf{g}}_0^T(\mathbf{y}_s, \omega) \widehat{V}_j(\omega)|^2}, \quad s = 1, \dots, K. \quad (\text{B.3})$$

We can interpret (B.3) in terms of the images created by the singular vectors having zero singular value, as $\widehat{\mathbf{g}}_0^T(\mathbf{y}_s, \omega) \widehat{V}_j(\omega)$ is the incident field at the search point \mathbf{y}_s due to a illumination vector $\widehat{V}_j(\omega)$ on the array. According to this interpretation, the singular vectors having zero singular value do not illuminate the scatterers locations and, hence, (B.3) has a peak when $\mathbf{y}_s = \mathbf{y}_{n_j}$.

Since in our application the number of scatterers is small, the signal space is much smaller than the noise space and, therefore, it is more efficient to compute the equivalent functional

$$\mathcal{I}_{MUSIC}(\mathbf{y}_s) = \frac{\min_{1 \leq j \leq K} \|\mathcal{P}\widehat{\mathbf{g}}_0(\mathbf{y}_j, \omega)\|_{\ell_2}}{\|\mathcal{P}\widehat{\mathbf{g}}_0(\mathbf{y}_s, \omega)\|_{\ell_2}}, \quad s = 1, \dots, K, \quad (\text{B.4})$$

with the projection onto the noise space defined as

$$\mathcal{P}\widehat{\mathbf{g}}_0(\mathbf{y}, \omega) = \widehat{\mathbf{g}}_0(\mathbf{y}, \omega) - \sum_{j=1}^M (\widehat{\mathbf{g}}_0^T(\mathbf{y}, \omega) \widehat{V}_j(\omega)) \widehat{V}_j(\omega). \quad (\text{B.5})$$

The numerator in (B.4) is just a normalization. We note that (B.4) is robust to noise, even for single frequency and for non-homogeneous, random media, and it is quite accurate for large arrays [2]. Generalizations of MUSIC for multiple scattering and extended scatterers have also been developed (see, for example, [17] and [19]).

REFERENCES

- [1] L. BORCEA AND I. KOCYIGIT, *Resolution analysis of imaging with ℓ_1 optimization*, SIAM J. Imaging Sci. 8 (2015), pp. 3015–3050.
- [2] L. BORCEA, C. TSOGKA, G. PAPANICOLAOU AND J. BERRYMAN, *Imaging and time reversal in random media*, Inverse Problems. 18 (2002), pp. 1247–1279.
- [3] E. CANDÈS AND T. TAO, *Decoding by linear programming* IEEE Trans. Inform. Theory 51 (2005), pp. 4203–4215.
- [4] E. CANDÈS AND B. RECHT, *Exact matrix completion via convex optimization* Foundations of Computational Mathematics 9, 6 (2009), pp. 717–772.
- [5] E. J. CANDÈS, Y. C. ELДАР, T. STROHMER, AND V. VORONINSKI, *Phase Retrieval via Matrix Completion*, SIAM Journal on Imaging Sciences 6 (2013), pp. 199–225.
- [6] A. CHAI, M. MOSCOSO AND G. PAPANICOLAOU, *Array imaging using intensity-only measurements*, Inverse Problems 27 (2011), 015005.

- [7] A. CHAI, M. MOSCOSO AND G. PAPANICOLAOU, *Robust imaging of localized scatterers using the singular value decomposition and ℓ_1 optimization*, Inverse Problems 29 (2013), 025016.
- [8] A. CHAI, M. MOSCOSO AND G. PAPANICOLAOU, *Imaging Strong Localized Scatterers with Sparsity Promoting Optimization*, SIAM J. Imaging Sci. 7 (2014), pp. 1358–1387.
- [9] E. CUCHE, P. MARQUET AND C. DEPEURSINGE, *Simultaneous amplitude-contrast and quantitative phase-contrast microscopy by numerical reconstruction of Fresnel off-axis holograms*, Appl. Opt. 38 (1999), pp. 6994–7001.
- [10] J.C. DAINTY, J.R. FIENUP, *Phase retrieval and image reconstruction for astronomy*, Chapter 7 in H. Stark, ed., Image Recovery: Theory and Application (Academic Press, New York, 1987), pp. 231–275.
- [11] D. L. DONOHO, P. B. STARK: Uncertainty principles and signal recovery. SIAM J. Appl. Math. 49 (1989), 906–931
- [12] D. DONOHO, M. ELAD AND V. TEMLYAKOV, *Stable recovery of sparse overcomplete representations in the presence of noise*, IEEE Trans. Information Theory 52 (2006), pp. 6–18.
- [13] A. FANNJIANG, *Absolute uniqueness of phase retrieval with random illumination*, Inverse Problems 28 (2012), 075008.
- [14] A. FANNJIANG AND W. LIAO, *Coherence pattern-guided compressive sensing with unresolved grids*, SIAM J. on Imaging Sci. 5 (2012), pp. 179–202.
- [15] J.R. FIENUP, *Phase retrieval algorithms: a comparison*, Applied Optics 21 (1982), pp. 2758–2768.
- [16] R. W. GERCHBERG AND W. O. SAXTON, *A practical algorithm for the determination of the phase from image and diffraction plane pictures*, Optik 35 (1972), pp. 237–246.
- [17] F. GRUBER, E. MARENGO AND A. DEVANEY, *Time-reversal imaging with multiple signal classification considering multiple scattering between the targets*, J. Acoust. Soc. Am. 115 (2004), pp. 3042–3047.
- [18] R.W. HARRISON, *Phase problem in crystallography*, J. Opt. Soc. Am. A 10 (1993), pp. 1046–1055.
- [19] S. HOU, K. SOLNA, AND H. ZHAO, *A direct imaging algorithm for extended targets*, Inverse Problems 22 (2006), pp. 1151–1178
- [20] R.P. MILLANE, *Phase retrieval in crystallography and optics*, J. Opt. Soc. Am. A 7 (1990), pp. 394–411.
- [21] A. NOVIKOV, M. MOSCOSO, G. PAPANICOLAOU, *Illumination strategies for intensity-only imaging*, SIAM Journal of Imaging Sci. 8 (2015), pp. 1547–1573.
- [22] F. PFEIFFER, T. WEITKAMP, O. BUNK AND C. DAVID, *Phase retrieval and differential phase-contrast imaging with low-brilliance X-ray sources*, Nature Physics 2 (2006), pp. 258–261.
- [23] R. O. SCHMIDT, *Multiple Emitter Location and Signal Parameter Estimation*, IEEE Trans. Antennas Propag. 34 (1986), pp. 276–280.
- [24] K. C. TOH AND S. YUN, *An accelerated proximal gradient algorithm for nuclear norm regularized least squares problems* Pacific J. Optimization 6 (2010), pp. 615–640.
- [25] R. TREBINO, D. J. KANE, *Using phase retrieval to measure the intensity and phase of ultrashort pulses: frequency-resolved optical gating*, J. Opt. Soc. Am. A 10 (1993), pp. 1101–1111.
- [26] J. M. RODENBURG, *Ptychography and related diffractive imaging methods*, in Advances in Imaging and Electron Physics, P. W. Hawkes, ed. (Elsevier, 2008), Vol. 150, pp. 87–184.
- [27] A. WALTHER, *The question of phase retrieval in optics*, Journal of Modern Optics 1 (1963), pp. 41–49.
- [28] I. YAMAGUCHI AND T. ZHANG, *Phase-shifting digital holography*, Opt. Lett. 22 (1997), pp. 1268–1270.